

An Ultrasensitive Nanowire-Transistor Biosensor for Detecting Dopamine Release from Living PC12 Cells under Hypoxic Stimulation

Bor-Ran Li,[†] Ying-Jhu Hsieh,[‡] Yan-Xi Chen,[‡] Ya-Ting Chung,[§] Chien-Yuan Pan,[§] and Yit-Tsong Chen^{*,†,‡}

[†]Institute of Atomic and Molecular Sciences, Academia Sinica, P.O. Box 23-166, Taipei 106, Taiwan

[‡]Department of Chemistry and [§]Department of Life Science, National Taiwan University, No. 1, Sec. 4, Roosevelt Road, Taipei 106, Taiwan

S Supporting Information

ABSTRACT: Dopamine (DA) is an important neurotransmitter that is involved in neuronal signal transduction and several critical illnesses. However, the concentration of DA is extremely low in patients and is difficult to detect using existing electrochemical biosensors with detection limits typically around nanomolar levels ($\sim 10^{-9}$ M). Here, we developed a nanoelectronic device as a biosensor for ultrasensitive and selective DA detection by modifying DNA-aptamers on a multiple-parallel-connected (MPC) silicon nanowire field-effect transistor (referred to as MPC aptamer/SiNW-FET). Compared with conventional electrochemical methods, the MPC aptamer/SiNW-FET has been demonstrated to improve the limit of DA detection to $< 10^{-11}$ M and to possess a detection specificity that is able to distinguish DA from other chemical analogues, such as ascorbic acid, catechol, phenethylamine, tyrosine, epinephrine, and norepinephrine. This MPC aptamer/SiNW-FET was also applied to monitor DA release under hypoxic stimulation from living PC12 cells. The real-time recording of the exocytotic DA induced by hypoxia reveals that the increase in intracellular Ca^{2+} that is required to trigger DA secretion is dominated by an extracellular Ca^{2+} influx, rather than the release of intracellular Ca^{2+} stores.

Dopamine (DA) is an important neurotransmitter that plays many important roles in the nervous, cardiovascular, and renal systems and regulates various physiological activities. When mammals do not have enough oxygen, their brains send out signals, through DA, to increase the breathing rate and blood circulation to reoxygenate the organs.¹ In addition to regulating physiological activities, DA is also related to several critical illnesses. In the basal ganglia of the brain, DA is a neurotransmitter that plays a vital role in Parkinson's disease, which is a notorious nervous dysfunction associated with vibrating limbs during the early stages and dementia in the advanced stages.² Schizophrenia has been shown to increase DA activity in the dopaminergic pathway and to reduce DA in the cortex.³ Clinically, an abnormal DA level in either the urine or blood indicates pheochromocytomas and paragangliomas,^{4,5} which are rare tumors arising in neural crest tissue. Consequently, quickly detecting and accurately quantifying DA levels is important for cellular investigation and biomedical diagnosis.

Among the existing tools that detect DA, electrochemical methods are dominant because of their speed and convenience. However, the oxidation potential of DA overlaps with that of many other substances in urine, blood, and the central nervous system (e.g., ascorbic acid (AA)). Moreover, the concentration of DA in the extracellular fluid of Parkinson's disease patients and in the urine/blood of patients with pheochromocytomas or paragangliomas is extremely low ($< 10^{-10}$ M)⁶ and very difficult to detect at the normal concentrations of a clinical sample using conventional electrochemical methods (typically with detection limits no better than nanomolar, as listed in Table S1 of the Supporting Information (SI)). Therefore, a new DA sensor with high detection sensitivity and target selectivity is highly desired.

Over the past decade, silicon nanowire field-effect transistors (SiNW-FETs) have attracted great attention for applications in ultrasensitive biomolecular detections.^{7–16} A SiNW has a large surface-to-volume ratio, which allows a small variation in the local charges on the wire surface to result in a significant conductance change inside the SiNW-FET due to an electric-field effect. SiNW-FETs modified with selected receptor molecules can be used as biosensors to detect specific targets in real-time with label-free, sensitive, and selective sensing. By judiciously selecting a suitable DA recognizer to attach to the SiNW-FET, these functionalized, nanoelectronic devices can be excellent biosensors for the highly sensitive and selective detection of DA.

The bioanalytes used for molecular recognition with SiNW-FETs are mostly large in size, have high molecular weights, and carry large charges, which can exert a strong electric field that facilitates detection by FETs.^{7,17} It is comparatively challenging for FET-based biosensors to recognize weakly charged, small molecules, such as DA. To date, only a few small molecules have been studied with SiNW-FETs (and/or carbon nanotube-FETs), e.g., the label-free detections of adenosine-5'-triphosphate¹⁸ and glutamate.¹⁹ For sensing DA in this study, we built a multiple-parallel-connected (MPC) SiNW-FET with greater reliability and higher sensitivity than a traditional single-channel SiNW-FET. This higher sensitivity is essential for recognition of weakly charged, small biomolecules.

As illustrated in Figure 1A, the electrical measurements of an MPC SiNW-FET were conducted with a lock-in amplifier, and

Received: August 16, 2013

Published: October 14, 2013

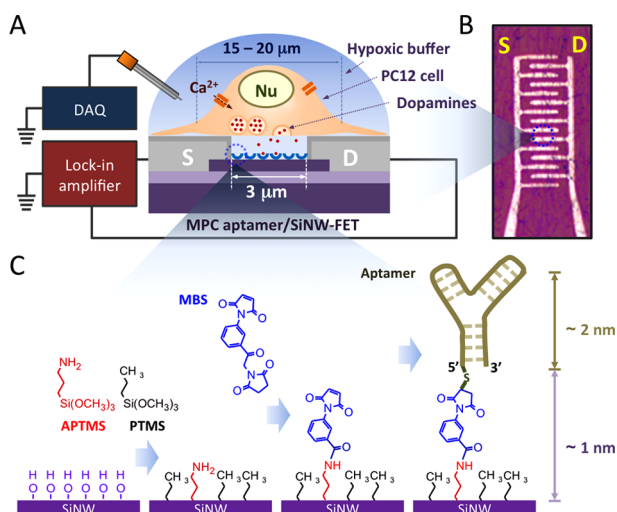


Figure 1. (A) Illustration of the experimental setup of a DNA-aptamer-modified MPC SiNW-FET device for detecting exocytotic DA under hypoxic stimulation from living PC12 cells. (B) Optical microscopy image of an MPC SiNW-FET device. S = source; D = drain. (C) Procedure for immobilization of the DNA-aptamer on an MPC SiNW-FET (details in sections S3 and S4 of the Supporting Information). Abbreviations: APTMS, (3-aminopropyl)trimethoxysilane; PTMS, propyltrimethoxysilane; MBS, 3-maleimidobenzoic acid *N*-hydroxysuccinimide ester. The drawing is not to scale.

the solution gate voltage was supplied by a data acquisition (DAQ) system through a platinum electrode. Details of the device fabrication and the electrical measurements of the MPC SiNW-FETs are described in sections S1–S5 of the SI. Each unit of the MPC SiNW-FET devices comprises hundreds of p-type single-crystalline SiNWs (~ 20 nm in diameter each) as conducting channels, which were connected by two sets of comb-like source and drain electrodes (Figure 1B and details in Figure S1A of the SI). Electrical characterizations of MPC SiNW-FETs reveal that the nanoelectronic devices have ohmic contacts (Figure S1B) and high transconductance with a typical value of 600 nS at a source–drain bias voltage (V_{sd}) of 10 mV (Figure S1C). Compared with a traditional SiNW-FET, whose conducting channel is composed of only a single or a few SiNWs, the MPC SiNW-FET system possesses remarkably higher detection sensitivity (i.e., larger transconductance) and a better signal-to-noise ratio (S/N) in electrical measurements (Figure S2).

In this work, we chose a DNA-aptamer^{20,21} with high specific binding to DA as the receptor to be modified on an MPC SiNW-FET. The immobilization of the DNA-aptamers was designed to modify only the SiNWs surface without contaminating the surrounding substrate of the FET chip, which substantially enhances the detection sensitivity, as we demonstrated earlier.^{22,23} The DNA-aptamer-modified MPC SiNW-FET (referred to as aptamer/SiNW-FET hereafter) has several advantages for molecular recognition by affinity-based biosensors. First, an aptamer has a smaller molecular size than conventional receptors (e.g., enzymes or antibodies); therefore, the captured DA molecules are closer to the SiNW-FET during the sensing measurement, resulting in a stronger electrical field exerted from the DA that modulates the conductance inside SiNW-FET and gives optimal detection signals. Second, an aptamer formed by oligonucleic acids is thermally stable. This stability is in sharp contrast to proteins and antibodies, which may lose their functionality irreversibly under thermal/chemical

attacks. Moreover, denatured aptamers are able to recover their function by self-refolding.

An artificial single-strain DNA oligonucleotide of 57-mer (HS-5'-GTC TCT GTG TGC GCC AGA GAC ACT GGG GCA GAT ATG GGC CAG CAC AGA ATG AGG CCC-3', synthesized by MDBio) was adopted as the aptamer for DA sensing. The sequence was *in vitro*-selected from random RNA pools²¹ and was confirmed to retain DA affinity in the DNA form.²⁰ Although the crystal structure of this DA binding aptamer is still unresolved, the tertiary structure, according to the biochemical data from previous research,²¹ should be highly compact and consists of two major stem-loop domains enclosing five DA binding sites (Figure S3). The immobilization procedures of the aptamers on an MPC SiNW-FET are illustrated schematically in Figure 1C (details in sections S3 and S4 of the SI). We first test the binding ability of the aptamer to various molecules including AA (which is the major interfering molecule present in cells and has a redox potential close to DA), catechol (CT) and phenethylamine (PEA) (structurally similar to DA), tyrosine (TR) (a biomolecule involved in the DA metabolism), and epinephrine (EP) and norepinephrine (NE) (other catecholamines).

Figure 2A plots the relationships between the source–drain current (I_{sd}) and the gate voltage (V_g) of an aptamer/SiNW-FET

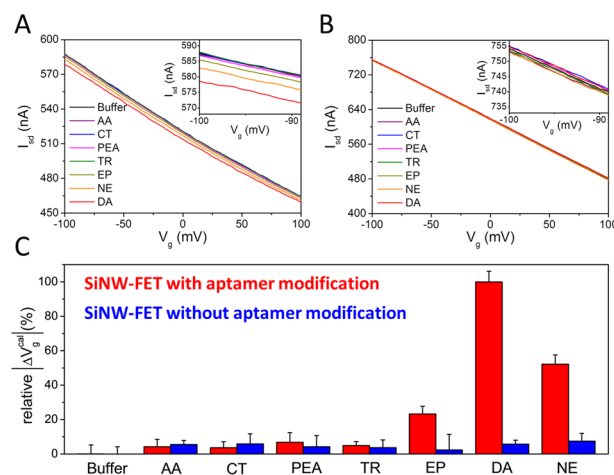


Figure 2. I_{sd} – V_g curves measured with (A) an aptamer/SiNW-FET and (B) a PTMS-modified SiNW-FET without aptamer modification (referred to as a bare SiNW-FET hereafter) for the detection of 0.1× PBS buffer, 1 μ M ascorbic acid (AA), 1 μ M catechol (CT), 1 μ M phenethylamine (PEA), 1 μ M tyrosine (TR), 10 nM epinephrine (EP), 10 nM dopamine (DA), and 10 nM norepinephrine (NE). (C) Calibrated responses (ΔI_{sd}^{cal}) of the various biochemicals relative to that of DA (100%). The error bars present the standard deviations of three measurements.

device in response to various molecules dissolved in 0.1× phosphate-buffered saline (PBS, composed of 13.7 mM NaCl, 270 μ M KCl, 1 mM Na_2HPO_4 , and 200 μ M KH_2PO_4 in NaOH, pH 7.2). While 10 nM DA caused a prominent shift of the I_{sd} – V_g curve, AA, CT, PEA, and TR at 1 μ M had little effect on the curves, and 10 nM of EP and NE induced limited changes. As a control test (Figure 2B), a bare SiNW-FET device without modification of the DNA-aptamer had no response to these molecules. To avoid variation among the different devices,²⁴ the measured current change due to the receptor–target binding (ΔI_{sd} at $V_g = -90$ mV, relative to the buffer solution in Figure 2A) was converted to the change in V_g (termed the calibrated

response and represented by $\Delta V_{g,DA}^{cal}$ as illustrated in Figure S4) according to the $I_{sd}-V_g$ transfer curve of the FET device used. Changes induced by the tested buffers containing AA (1 μ M), CT (1 μ M), PEA (1 μ M), TR (1 μ M), EP (10 nM), DA (10 nM), and NE (10 nM) are summarized in Figure 2C. Although those two catecholamines of EP and NE caused significant $\Delta V_{g,DA}^{cal}$ of $25 \pm 4\%$ and $50 \pm 5\%$, respectively, all other non-catecholamines induced changes less than 10% despite the 100-fold greater concentration that was used. These results indicate the specificity of the DNA-aptamer in distinguishing catecholamines from other molecules. Moreover, the association of DA with an aptamer of mutations at the binding sites (referred to as mut-aptamer) is very weak as shown in Figure S5, where 10 nM DA induced only a small change of $\Delta V_{g,DA}^{cal} < 10\%$ in a mut-aptamer/SiNW-FET.

We next determined the binding affinity of the DNA-aptamer to various catecholamines. The test was carried out with the analytes at 10^{-13} – 10^{-7} M in $0.1\times$ PBS. Figure 3A shows the $I_{sd}-V_g$

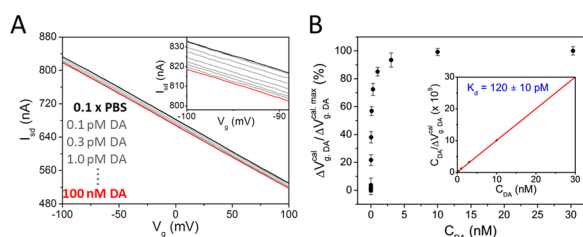


Figure 3. (A) Measured $I_{sd}-V_g$ curves of an aptamer/SiNW-FET in response to different DA concentrations ($C_{DA} = 0-100$ nM in $0.1\times$ PBS at pH 7.2). The magnified scale is shown in the inset. (B) Normalized plot of $\Delta V_{g,DA}^{cal}/\Delta V_{g,DA}^{cal,max}$ (where $\Delta V_{g,DA}^{cal,max}$ is the saturated $\Delta V_{g,DA}^{cal}$) as a function of C_{DA} is summarized from the data in (A). The inset shows the least-squares fit to the Langmuir adsorption isotherm model (section S6 of the SI), yielding $K_d = 120 \pm 10$ pM for the aptamer-DA complex.

V_g plots of the aptamer/SiNW-FET measured at various DA concentrations (C_{DA}), where the data were subsequently converted to the calibrated response ($\Delta V_{g,DA}^{cal}$) as a function of C_{DA} in Figure 3B. The inset in Figure 3B plots the $C_{DA}/\Delta V_{g,DA}^{cal}$ against various C_{DA} , and the dissociation constant (K_d) of the aptamer-DA complex was 120 ± 10 pM, which was determined from the least-squares fit to the Langmuir adsorption isotherm model (details in section S6 of the SI).^{7,22} As displayed in Figure S6, the linear working range of the aptamer/SiNW-FET biosensor for DA detection spanned from 10^{-11} to 10^{-8} M. Similarly, the K_d values of the aptamer-EP and aptamer-NE complexes were 6.03 ± 1.85 nM and 910 ± 270 pM, respectively (Figure S7). These data show that the affinity of the DNA-aptamer for DA is approximately 50- and 10-fold over EP and NE, respectively. Because of this affinity for DA and additional biological DA in some living systems (e.g., PC12 cells contain 10-fold more DA than other catecholamines²⁵ and dopaminergic neurons synthesize exclusively DA), this aptamer/SiNW-FET can be used as a unique biosensor for practical DA detection in cellular investigation and clinical diagnosis.

In addition to selectivity and sensitivity, real-time detection allows the SiNW-FET biosensor to monitor the cellular response to drug treatment or environmental alteration. Although many time-dependent measurements using techniques that do not have real-time responses have been used to detect the DA release from cells, these measurements usually require hours of work for sample collection and DA recognition using HPLC purification and mass identification. In comparison, Figure 4A shows a

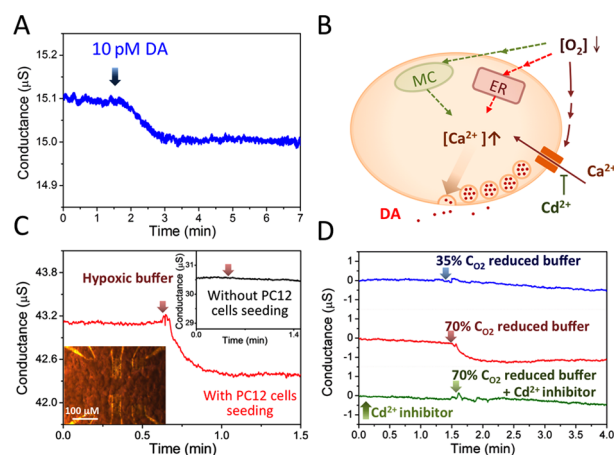


Figure 4. (A) Real-time recording of 10 pM DA by aptamer/SiNW-FET. The analytes were driven by a micropump (0.3 mL/h) through a PDMS microfluidic channel. (B) Illustration of a hypothetical mechanism of cellular DA secretion under hypoxic stimulation. The escalation of intracellular Ca^{2+} to trigger DA exocytosis is speculated to occur via the pathway of either extracellular Ca^{2+} influx (solid lines)²⁰ or intracellular Ca^{2+} store release²¹ (dashed lines). (C) Real-time recording of PC12 cells that are seeded with aptamer/SiNW-FET (bottom inset: optical microscopy image) in response to the addition of 70% CO_2 reduced hypoxic buffer (section S8 of the SI). Top inset shows a control test using the same aptamer/SiNW-FET but without cells seeding. Arrows indicate the addition of hypoxic buffer. (D) Real-time recordings of the DA release from PC12 cells under different hypoxic stimulations: (upper trace) 35% CO_2 reduced buffer, (middle trace) 70% CO_2 reduced buffer, and (bottom trace) 70% CO_2 reduced buffer containing 1 mM CdI_2 .

representative real-time recording using an aptamer/SiNW-FET, where 10 pM DA was detected ($S/N > 5$) with a conductance change of ~ 100 nS within 1.5 min at a flow rate of 0.3 mL/h. In a further test of the aptamer/SiNW-FET, we attempted to conduct real-time recordings of the DA release under hypoxic stimulation from living PC12 cells.

For mammalian cells, adequate oxygen is essential for their survival; therefore, mammals undergo hypoxia-induced cellular processes to tolerate an oxygen deprivation environment. Such examples include the release of transmitters from neuronal cells. The hypoxic effect on PC12 cells induces the release of DA through exocytosis, which involves an increase in intracellular Ca^{2+} in the stimulus–secretion coupling.²⁶ However, the cellular mechanism of coupling hypoxic stimulation with DA secretion is complicated; whether the pathway involved in increasing intracellular Ca^{2+} and triggering DA exocytosis via either extracellular Ca^{2+} influx²⁷ or release of intracellular Ca^{2+} stores²⁸ (as illustrated in Figure 4B) is still under debate. In this test, we tried to apply the aptamer/SiNW-FET to resolve these controversial pathways. The experimental setup of an aptamer/SiNW-FET for real-time recording of the exocytotic DA under hypoxic stimulation from living PC12 cells is illustrated in Figure 1A, where PC12 cells cultured in a polydimethylsiloxane (PDMS) well (section S7 of the SI) were applied directly on the SiNW-FET device (bottom inset of Figure 4C). As shown in Figure 4C, a progressive increase in the DA efflux was recorded while the PC12 cells suffered from a hypoxia of a 70% decrease in the environmental O_2 concentration (CO_2); meanwhile, the increase in DA reached equilibrium within 0.5 min. As a control experiment, no significant change in electrical conductance was

observed with an aptamer/SiNW-FET without cell seeding (upper inset of Figure 4C). Moreover, the DA release by hypoxic stimulation is not linearly correlated to the reduced CO_2 , where the exocytotic DA could not be detected until the CO_2 was reduced by more than 70% (Figure 4D). This observation indicates that the deoxygenization via minor hypoxic stimulation (e.g., 35% reduced CO_2) is not sufficient to trigger the membrane potential depolarization, leading to the activation of the voltage-gated Ca^{2+} channels to elevate the intracellular Ca^{2+} concentration and trigger neurotransmitter release. In addition, after the Ca^{2+} channels had been blocked by cadmium ions (by adding 1 mM CdI_2), PC12 cells failed to release DA in spite of hypoxic stimulation (Figure 4D). These results reveal that the increase in intracellular Ca^{2+} that triggers the DA secretion following hypoxic stimulation is dominated by the influx of extracellular Ca^{2+} .

In summary, an MPC aptamer/SiNW-FET was demonstrated for the first time to be a reliable DA sensor. Furthermore, the nanoelectronic biosensor possesses the advantages of high sensitivity and selectivity and can be used in real-time, label-free detections. The MPC aptamer/SiNW-FET has a strong binding affinity for DA that is at least 10-fold over the rival catecholamines of NE and EP; these three catecholamines could not be discerned using conventional electrochemical methods. The ultrasensitive MPC aptamer/SiNW-FET, capable of probing DA down to 10^{-11} M, can be used as a practical biosensor to detect DA at the extremely low concentration level ($<10^{-10}$ M) in the extracellular fluid of Parkinson's disease patients and in the urine/blood of patients with pheochromocytomas or paragangliomas.⁶ Using this MPC aptamer/SiNW-FET for DA detection, we have successfully monitored DA release from living PC12 cells following hypoxia-induced cellular secretion. DA secretion following hypoxic stimulation has been verified to be coupled with extracellular Ca^{2+} influx. Finally, this novel bionanoelectronic device, which is capable of integrating with living cell systems, adds a new item to the biosensor toolbox for the future studies of cell biology and clinical disease diagnosis.

■ ASSOCIATED CONTENT

📄 Supporting Information

Figures S1–S8 and methods. This material is available free of charge via the Internet at <http://pubs.acs.org>.

■ AUTHOR INFORMATION

Corresponding Author

ytchem@ntu.edu.tw

Notes

The authors declare no competing financial interest.

■ ACKNOWLEDGMENTS

This work was partially supported by the National Science Council of Taiwan under NSC 101-2627-M-002-004 and 101-2627-M-002-013. B.-R.L. was supported by a postdoctoral fellowship from Academia Sinica. Technical support from NanoCore, the Core Facilities for Nanoscience and Nanotechnology at Academia Sinica, is acknowledged.

■ REFERENCES

- (1) Urena, J.; Fernandezchacon, R.; Benot, A. R.; Detoledo, G. A.; Lopezbarneo, J. *Proc. Natl. Acad. Sci. U.S.A.* **1994**, *91*, 10208.
- (2) Kim, J. H.; Auerbach, J. M.; Rodriguez-Gomez, J. A.; Velasco, I.; Gavin, D.; Lumelsky, N.; Lee, S. H.; Nguyen, J.; Sanchez-Pernaute, R.; Bankiewicz, K.; McKay, R. *Nature* **2002**, *418*, 50.
- (3) Meyer-Lindenberg, A.; Miletich, R. S.; Kohn, P. D.; Esposito, G.; Carson, R. E.; Quarantelli, M.; Weinberger, D. R.; Berman, K. F. *Nat. Neurosci.* **2002**, *5*, 267.
- (4) Pacak, K.; Eisenhofer, G.; Ahlman, H.; Bornstein, S. R.; Gimenez-Roqueplo, A. P.; Grossman, A. B.; Kimura, N.; Mannelli, M.; McNicol, A. M.; Tischler, A. S. *Nat. Clin. Pract. Endocrinol.* **2007**, *3*, 92.
- (5) Eisenhofer, G.; Goldstein, D. S.; Sullivan, P.; Csako, G.; Brouwers, F. M.; Lai, E. W.; Adams, K. T.; Pacak, K. *J. Clin. Endocrinol. Metab.* **2005**, *90*, 2068.
- (6) Davis, K. L.; Kahn, R. S.; Ko, G.; Davidson, M. *Am. J. Psychiatry* **1991**, *148*, 1474.
- (7) Chen, K. I.; Li, B. R.; Chen, Y. T. *Nano Today* **2011**, *6*, 131.
- (8) Cui, Y.; Wei, Q. Q.; Park, H. K.; Lieber, C. M. *Science* **2001**, *293*, 1289.
- (9) Bunimovich, Y. L.; Shin, Y. S.; Yeo, W.-S.; Amori, M.; Kwong, G.; Heath, J. R. *J. Am. Chem. Soc.* **2006**, *128*, 16323.
- (10) Stern, E.; Klemic, J. F.; Routenberg, D. A.; Wyrembak, P. N.; Turner-Evans, D. B.; Hamilton, A. D.; LaVan, D. A.; Fahmy, T. M.; Reed, M. A. *Nature* **2007**, *445*, 519.
- (11) Lin, T. W.; Hsieh, P. J.; Lin, C. L.; Fang, Y. Y.; Yang, J. X.; Tsai, C. C.; Chiang, P. L.; Pan, C. Y.; Chen, Y. T. *Proc. Natl. Acad. Sci. U.S.A.* **2010**, *107*, 1047.
- (12) Lin, S. P.; Pan, C. Y.; Tseng, K. C.; Lin, M. C.; Chen, C. D.; Tsai, C. C.; Yu, S. H.; Sun, Y. C.; Lin, T. W.; Chen, Y. T. *Nano Today* **2009**, *4*, 235.
- (13) Gao, X. P. A.; Zheng, G. F.; Lieber, C. M. *Nano Lett.* **2010**, *10*, 547.
- (14) Zhang, G. J.; Chua, J. H.; Chee, R. E.; Agarwal, A.; Wong, S. M. *Biosens. Bioelectron.* **2009**, *24*, 2504.
- (15) Pui, T. S.; Agarwal, A.; Ye, F.; Huang, Y. X.; Chen, P. *Biosens. Bioelectron.* **2011**, *26*, 2746.
- (16) Zheng, G. F.; Patolsky, F.; Cui, Y.; Wang, W. U.; Lieber, C. M. *Nat. Biotechnol.* **2005**, *23*, 1294.
- (17) Zayats, M.; Huang, Y.; Gill, R.; Ma, C. A.; Willner, I. *J. Am. Chem. Soc.* **2006**, *128*, 13666.
- (18) Wang, W. U.; Chen, C.; Lin, K. H.; Fang, Y.; Lieber, C. M. *Proc. Natl. Acad. Sci. U.S.A.* **2005**, *102*, 3208.
- (19) Lee, G. J.; Lim, J. E.; Park, J. H.; Choi, S. K.; Hong, S.; Park, H. K. *Curr. Appl. Phys.* **2009**, *9*, S25.
- (20) Walsh, R.; DeRosa, M. C. *Biochem. Biophys. Res. Commun.* **2009**, *388*, 732.
- (21) Mannironi, C.; DiNardo, A.; Fruscoloni, P.; TocchiniValentini, G. *Biochemistry* **1997**, *36*, 9726.
- (22) Li, B. R.; Chen, C. W.; Yang, W. L.; Lin, T. Y.; Pan, C. Y.; Chen, Y. T. *Biosens. Bioelectron.* **2013**, *45*, 252.
- (23) Lin, T. Y.; Li, B. R.; Tsai, S. T.; Chen, C. W.; Chen, C. H.; Chen, Y. T.; Pan, C. Y. *Lab Chip* **2013**, *13*, 676.
- (24) Ishikawa, F. N.; Curreli, M.; Chang, H. K.; Chen, P. C.; Zhang, R.; Cote, R. J.; Thompson, M. E.; Zhou, C. W. *ACS Nano* **2009**, *3*, 3969.
- (25) Ahnert-Hilger, G.; Brautigam, M.; Gratzl, M. *Biochemistry* **1987**, *26*, 7842.
- (26) Kumar, G. K.; Overholt, J. L.; Bright, G. R.; Hui, K. Y.; Lu, H. W.; Gratzl, M.; Prabhakar, N. R. *Am. J. Physiol.-Cell Physiol.* **1998**, *274*, C1592.
- (27) Miao, Y. L.; Stein, P.; Jefferson, W. N.; Padilla-Banks, E.; Williams, C. J. *Proc. Natl. Acad. Sci. U.S.A.* **2012**, *109*, 4169.
- (28) Syntichaki, P.; Tavernarakis, N. *Nat. Rev. Neurosci.* **2003**, *4*, 672.

[Supporting Information]

An Ultra-Sensitive Nanowire-Transistor Biosensor for Detecting Dopamine Release from Living PC12 Cells under Hypoxic Stimulation

Bor-Ran Li,[†] Ying-Jhu Hsieh,[‡] Yan-Xi Chen,[‡] Ya-Ting Chung,^{||} Chien-Yuan Pan,^{||} and
Yit-Tsong Chen^{†‡*}

[†] Institute of Atomic and Molecular Sciences, Academia Sinica, P.O. Box 23-166, Taipei 106, Taiwan

[‡] Department of Chemistry, National Taiwan University, No. 1, Sec. 4, Roosevelt Road, Taipei 106, Taiwan

^{||} Department of Life Science, National Taiwan University, No. 1, Sec. 4, Roosevelt Road, Taipei 106, Taiwan.

S1. Materials and reagents

Deionized (DI) water ($>18\text{ M}\Omega\cdot\text{cm}$) obtained from a purification system (Millipore Synergy) was used throughout the experiments. The phosphate buffered saline ($1\times\text{PBS}$), consisting of 137 mM NaCl, 2.7 mM KCl, 10 mM Na_2HPO_4 , and 2 mM KH_2PO_4 in NaOH at pH 7.4, was purchased from Gibco. The chemicals 3-aminopropyl trimethoxysilane (APTMS), propyl trimethoxysilane (PTMS), dimethyl sulfoxide (DMSO), and 3-maleimidobenzoic acid N-hydroxy succinimide ester (MBS) were purchased from Sigma-Aldrich. Other chemicals were also purchased commercially: dithiothreitol (DTT) from J. T. Baker, the single-strain DNA-aptamer from MDBio, and polydimethylsiloxane (PDMS) from Sil-More Industrial.

S2. SiNW synthesis

Single-crystalline boron-doped SiNWs (Si:B = 4000:1) were synthesized catalytically with the assistance of 20 nm gold nanoparticles in a chemical vapor deposition (CVD) reaction through the vapor-liquid-solid (VLS) growth mechanism. Gold nanoparticles were dispersed onto a Si wafer chip with a 400-nm oxide layer that had been incubated in 0.1% aqueous solution of poly l-lysine for 10 min to increase the adhesion of the gold nanoparticles. After the deposition of gold nanoparticles, the substrate was washed with DI water, blown dry with N_2 gas, and cleaned in oxygen plasma (100 W and 50 sccm O_2 for 300 s). The p-type SiNWs were grown from the CVD reaction at 460 °C for 12.5 min in 10 sccm Ar, 6 sccm SiH_4 (10% in He), and 15 sccm B_2H_6 (100 ppm in He) at a total chamber pressure of 25 torr. The diameters of the as-synthesized SiNWs were generally between 20 and 30 nm. The quality of the as-synthesized SiNWs was examined using high-resolution transmission electron microscopy (HR-TEM) and electron diffraction (ED) (JEM-2000FXII). The experimental details of SiNW synthesis can be found in Refs. S1-S4.

S3. Device fabrication

Using a bottom-up technique, we fabricated selective surface modified (SSM) SiNW-FETs with the receptors modifying only the SiNW surface without contaminating the surrounding substrate of the Si wafer chip. The SSM SiNW-FETs can substantially increase their detection sensitivity, in comparison with the traditional all area modification (AAM) SiNW-FETs. In this approach, the strategy was to modify the SiNWs with a chemical linker of APTMS using a thermal-evaporation method prior to photolithographic fabrication of the device. The experimental details of the thermal-evaporation method can be found in Ref. S2. Briefly, a Si-wafer chip containing the as-synthesized SiNWs was

suspended in a sealed three-neck flask, which was pre-loaded with a 1:9 (v/v) solution of APTMS and PTMS. The flask was evacuated for 1 min at room temperature and incubated for 1 hr at 40 °C; meanwhile, the thermally evaporated APTMS and PTMS molecules were immobilized on the SiNW surface to form APTMS-modified SiNWs. On average, only ~10% of the SiNW surface contains APTMS as the active sites (amine groups) to be modified with aptamers (~2 nm in size). The modified PTMS on the 90% SiNW surface was used to not only adjust the density of the immobilized APTMS to avoid the steric hindrance of the immobilized aptamers, but also form a chemically inert surface to prevent non-specific binding in the later biosensing measurements.

The as-prepared APTMS-modified SiNWs were transferred onto a photoresist (S1805)-patterned Si wafer with a 400-nm oxide layer using a contact printing method. The SiNW-FET devices were fabricated following standard photolithographic procedures. The metal contact regions (defined by photolithography) were cleaned with oxygen plasma (100 sccm and 30 W); meanwhile, the native silica sheath of a SiNW in the contact area was removed with a buffered oxide etching (BOE) solution. Metal layers (70 nm Ni and 100 nm Al) were deposited consecutively using thermal evaporation on the areas defined by the pattern. The separation between the source and drain electrodes is 3 μm. After liftoff, the SiNW-FET devices were further annealed in forming gas (10% H₂ and 90% N₂) at 360 °C for 3 min to ensure good electrical contact between the SiNW and the metal electrodes.

S4. Immobilization of the aptamer

To anchor DNA-aptamers on the APTMS-modified SiNW-FETs, the chip containing the APTMS-modified SiNW-FET devices was immersed for 30 min in a 1:9 (v/v) solution of DMSO and 1× PBS containing 1 mM MBS. After the MBS had reacted with APTMS through the formation of an amide bond, the chip was rinsed with DI water, blown dry with N₂ gas, and immersed for 1 hr in a solution of 1× PBS containing 1 μM DNA-aptamer (disulfate DNA-dimer) and 100 mM DTT. After the sulfhydryl group of the DNA-aptamer had reacted with the maleimide group of MBS to immobilize the DNA-aptamer on the APTMS/SiNW-FETs (forming aptamer/SiNW-FETs), the chip was washed again with 1× PBS and DI water, and finally, blown dry with N₂ gas. To demonstrate the successful immobilization of DNA-aptamers on SiO₂/Si surface, we used FITC-tagged aptamer (5'-HS-GTC TCT GTG TGC GCC AGA GAC ACT GGG GCA GAT ATG GGC CAG CAC AGA ATG AGG CCC-FITC-3', referred to as FITC-aptamer) to show that the FITC-aptamers can be nicely immobilized on a SiO₂/Si substrate via the chemical linkers of MBS and APTMS (with the same modification process presented in Fig. 1C). Like the fluorescent images shown in Fig. S8A, while the FITC-aptamer could not be modified directly on a bare SiO₂/Si substrate (left panel, no fluorescence), the FITC-aptamers were effectively immobilized on a MBS/APTMS-modified SiO₂/Si substrate (right panel,

strong green fluorescence). The homogenous, uniform fluorescence image indicates the excellent modification of FITC-aptamers on the SiO₂/Si surface. The modification of DNA-aptamers on a SiNW-FET can also be examined by measuring the shift in the source-drain current vs. gate voltage ($I_{sd}-V_g$) curves. As depicted in Fig. S8B, the shift of the $I_{sd}-V_g$ curve after the DNA-aptamer modification is caused by a gating effect on the SiNW-FET due to the negatively charged DNA-aptamers, consequently increasing the conductance of the p-type SiNW-FET.

S5. Electrical measurement

In the electrical measurements of SiNW-FETs (Fig. 1), the source-drain current vs. gate voltage ($I_{sd}-V_g$) and the I_{sd} as a function of elapsed time ($I_{sd}-t$) were acquired with a lock-in amplifier (Stanford Research System, SR830) at $V_{sd} = 10$ mV, a modulation frequency of 79 Hz, and a time constant of 100 ms. In the biosensing measurements, the samples were dissolved in 0.1× PBS (Debye-Hückel length = 2.4 nm) allowing SiNW-FETs to effectively detect signals without severe electrolytic screening. The sample solution was either dropped directly onto the SiNW-FET devices, or delivered to the sensing devices through a polydimethylsiloxane (PDMS) microfluidic channel (6.26 mm (length) × 500 μm (width) × 50 μm (height)) driven by a syringe pump (KD-101, KD Scientific). A platinum electrode, immersed in the sample solution, was used as a solution gate with the voltage supplied by a data acquisition system (National Instruments, DAQ-NI2110) and was maintained at ground potential to minimize electrical noise throughout the real-time electrical measurements.^{S2-S11}

S6. Dissociation constant

The dissociation constant (K_d) of the aptamer–DA complex was determined by a least-squares fit of the $\Delta V_{g,DA}^{cal} - C_{DA}$ data (Fig. 3B) to the Langmuir adsorption isotherm model^{S2}

$$\frac{C_{DA}}{\Delta V_{g,DA}^{cal}} = \frac{1}{\Delta V_{g,DA}^{cal,max}} \cdot C_{DA} + \frac{1}{\Delta V_{g,DA}^{cal,max}} \cdot K_d, \quad (\text{Eq. S1})$$

where the relative $\Delta V_{g,DA}^{cal}$ is defined as $\Delta V_{g,DA}^{cal} (\%) = (\Delta V_{g,DA}^{cal} - \Delta V_{g,0}^{cal}) / \Delta V_{g,0}^{cal} \times 100(\%)$, $\Delta V_{g,0}^{cal}$ is the calibrated response at $C_{DA} = 0$ that induces no detectable signal, and $\Delta V_{g,DA}^{cal,max}$ is the saturated calibrated response at high C_{DA} .

S7. Culture PC12 Cells on SiNW-FET devices

The PC12 cell line, derived from pheochromocytoma of the rat adrenal medulla, was cultured in Dulbecco's modified Eagle's medium (containing 10% horse serum and 5% fetal bovine serum, Invitrogen) at 37 °C in an atmosphere containing 10% CO₂, and the medium was changed every other

day.^{S2,S12} Cultured cells were re-suspended with Eagle's medium and reseeded into a PDMS well directly on the aptamer/SiNW-FET devices at 37 °C for 2 hr. Before electrical measurements, the cultured cells were gently washed with 1× PBS buffer three times.

S8. Oxygen reduced buffers

In this work, anaerobic buffer was prepared by continuously bubbling 0.1× PBS buffer, sealed in a clean glass flask, with pure N₂ gas (purity: 5N) through a steel needle for 15 min. Buffer prepared in this way is a fully deoxygenized buffer that does not oxidize reduced methyl viologen (blue) to the oxidized form (colorless). Subsequently, various C_{O2} reduced buffers were prepared by volume-to-volume mixing the aerobic and anaerobic buffers.

Table S1. Comparison of the detection limits of various DA biosensors

Biosensing technique	Material	Surface modification	Linear working range (M)	Detection limit (M)	Ref.
Electrochemical detection	Glassy carbon	TNT	$10^{-7} - 10^{-5}$	10^{-7}	[S13]
	PET	Au nanowires	$10^{-7} - 10^{-4}$	10^{-8}	[S14]
	Carbon fiber	Tyrosinase	$10^{-8} - 10^{-4}$	10^{-9}	[S15]
	ITO	CNT	$10^{-8} - 10^{-6}$	10^{-8}	[S16]
	Graphene	Porphyrin	$10^{-8} - 10^{-5}$	10^{-8}	[S17]
Field-effect transistor	SiNW	Aptamer	$10^{-11} - 10^{-8}$	10^{-11}	This work

TNT: titanate nanotubes; PET: polyethylene terephthalate; ITO: indium tin oxide; CNT: carbon nanotube; SiNW: silicon nanowire

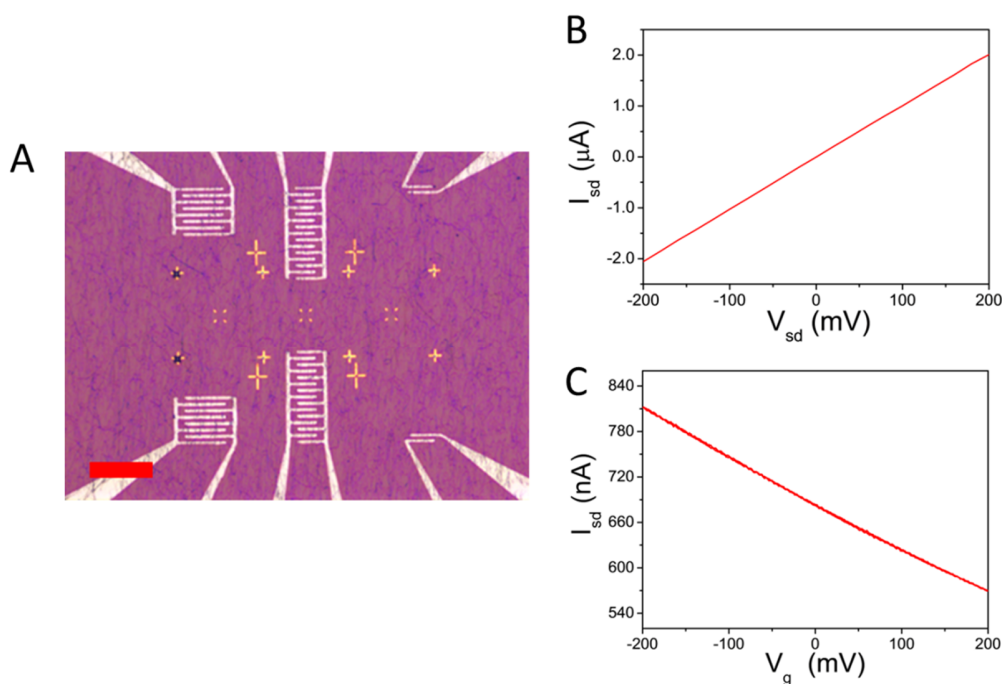


Figure S1. (A) Bright-field optical microscopy image of an MPC SiNW-FET device. Scale bar is 20 μm . The FET device contains six pairs of FET units, where four FET units (at the left-side) consisting of comb-like electrodes (MPC-system) were employed for experiments, and the other two FET units (at the right-side) containing two parallel electrodes were used as a control for comparison. Each MPC-FET unit comprises hundreds of p-type single-crystalline SiNWs (~ 20 nm in diameter each) as conducting channels, which were connected by two sets of comb-like source and drain electrodes. (B) A representative plot of the measured source-drain current as a function of the bias voltage (I_{sd} – V_{sd}) shows that MPC SiNW-FETs form ohmic contacts. The I_{sd} – V_{sd} curves were scanned in ambient condition with a digital multimeter (Keithley 6487). (C) The source-drain current vs. the gate voltage (I_{sd} – V_g) plot of a bare MPC SiNW-FET shows that the FET-device is of high transconductance with a typical value of >600 nS as measured in $0.1\times$ PBS buffer at $V_{sd} = 10$ mV. The I_{sd} – V_g measurement was conducted with a lock-in amplifier (Stanford Research System, SR830) at $V_{sd} = 10$ mV, a modulation frequency of 79 Hz, and a time constant of 100 ms. The V_g was scanned with a data acquisition system (National Instruments, DAQ BNC-2110) via an Ag/AgCl reference electrode.

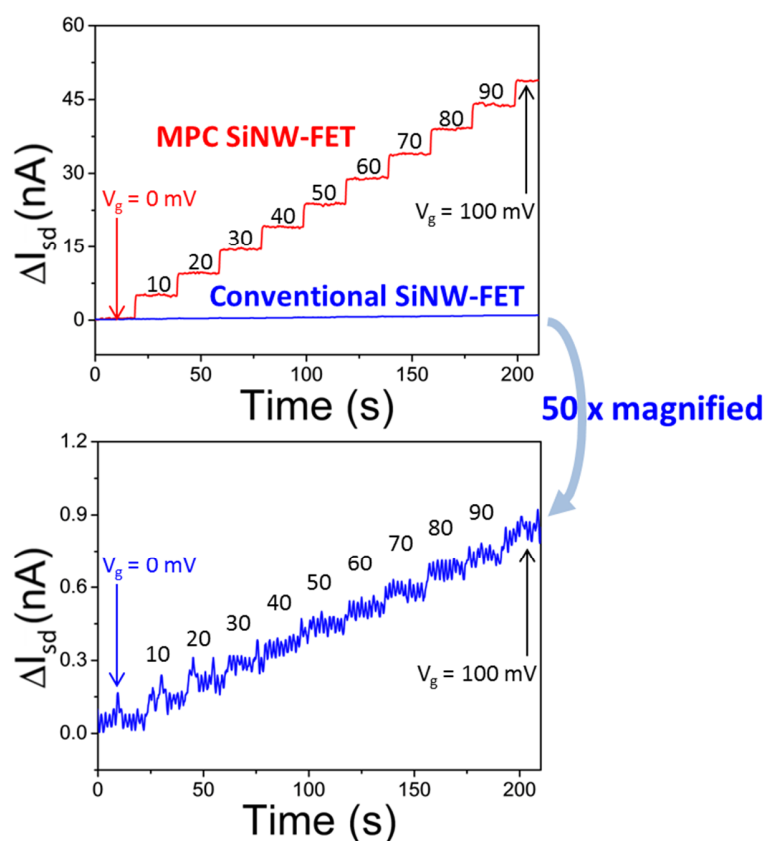


Figure S2. Comparison of the detection sensitivities of a MPC SiNW-FET (red trace) and a conventional SiNW-FET with a conducting channel consisting of only a single SiNW (blue trace). The ΔI_{sd} vs. elapse time plots were measured as a function of applied (solution) gate voltage (V_g). The V_g was applied through an Ag/AgCl reference electrode from 0 to 100 mV with an increasing rate of 10 mV/step. Signal acquisition of the electrical measurements was conducted with that lock-in amplifier described in S5. Relative to the measurement by conventional SiNW-FET, a significant improvement (more than 100-fold) in the S/N ratio of the signals measured by MPC SiNW-FET is clearly observed.

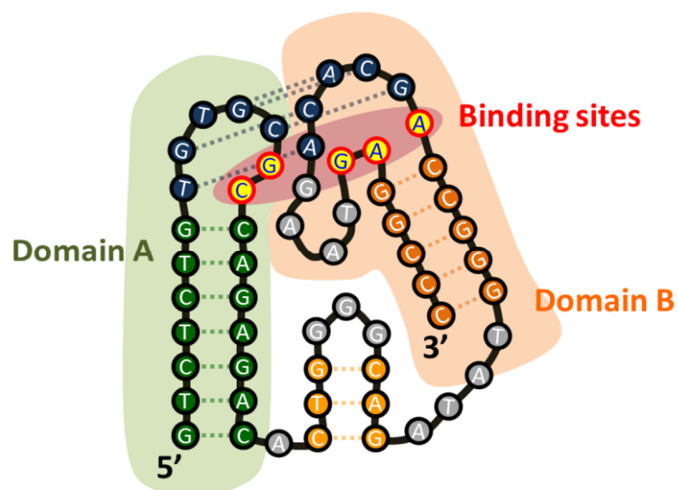


Figure S3. A schematic representation of the structure of the DNA-aptamer, which contains two major stem-loop domains (Domain A and Domain B) inclosing five DA binding sites on the loops (2 on Domain A and 3 on Domain B). The interaction of the two loops is indicated by the blue dashed lines.^{S18}

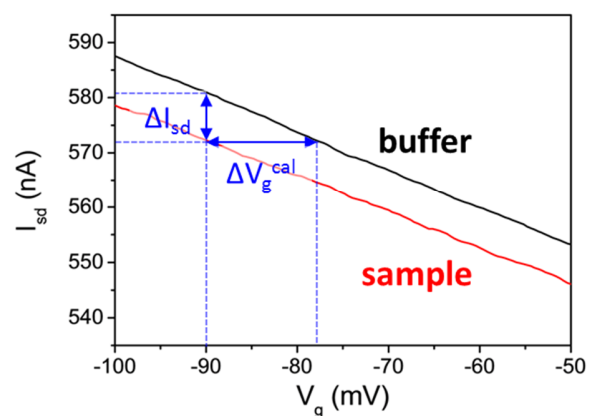


Figure S4. To avoid device-to-device variation in the detection sensitivity with different FETs, the measured current change due to the receptor-target binding (ΔI_{sd} at $V_g = -90$ mV, relative to the buffer solution) was converted to the change in V_g (termed the calibrated response and represented by ΔV_g^{cal}) according to the I_{sd} - V_g transfer curve of the FET device used.^{S2,S19}

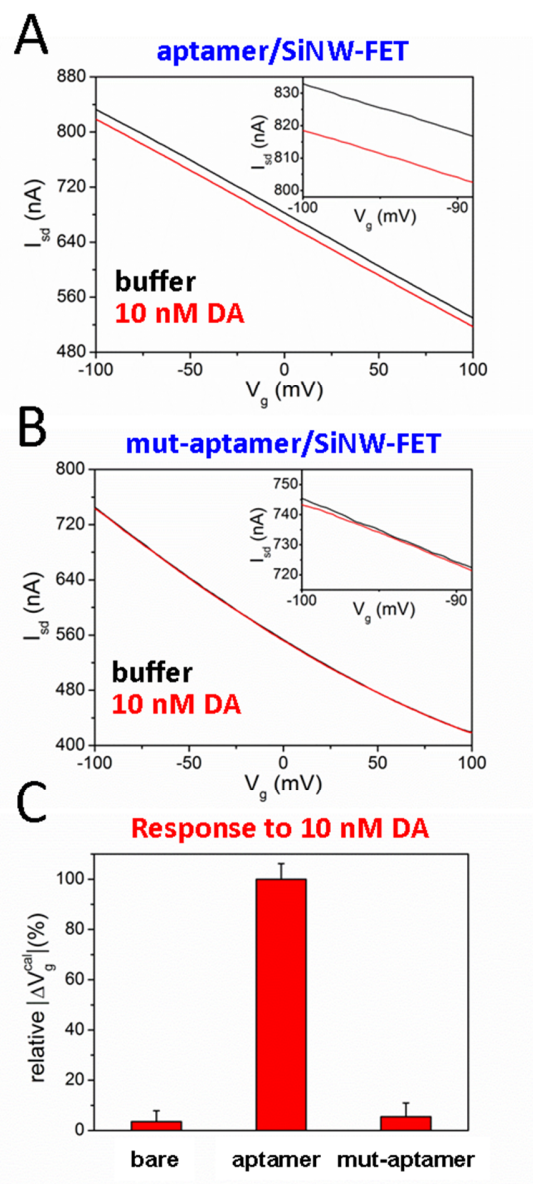


Figure S5. The I_{sd} - V_g curves measured with (A) an aptamer/SiNW-FET and (B) a mut-aptamer SiNW-FET for the detection of 10 nM DA in 0.1× PBS buffer. (C) A comparison of the calibrated responses (ΔV_g^{cal}) of a bare SiNW-FET and a mut-aptamer/SiNW-FET to that of an aptamer/SiNW-FET (100%). The error bars present the standard deviations of three measurements. The sequence of the mutated aptamer is 5'-GTC TCT GTG TGC AAC AGA GAC ACT GGG GCA GAT ATG GGC CTG CAC AGA ATT T TGG CCC-3'.

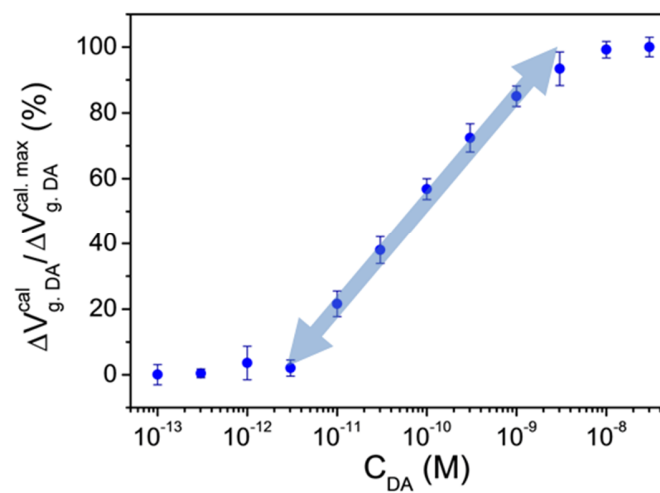


Figure S6. A semi-log plot of $\Delta V_{g,DA}^{cal} / \Delta V_{g,DA}^{cal,max}$ as a function of C_{DA} . The linear working range for detecting DA by aptamer/SiNW-FET spans from approximately 10^{-11} to 10^{-8} M, as marked by the double arrows.

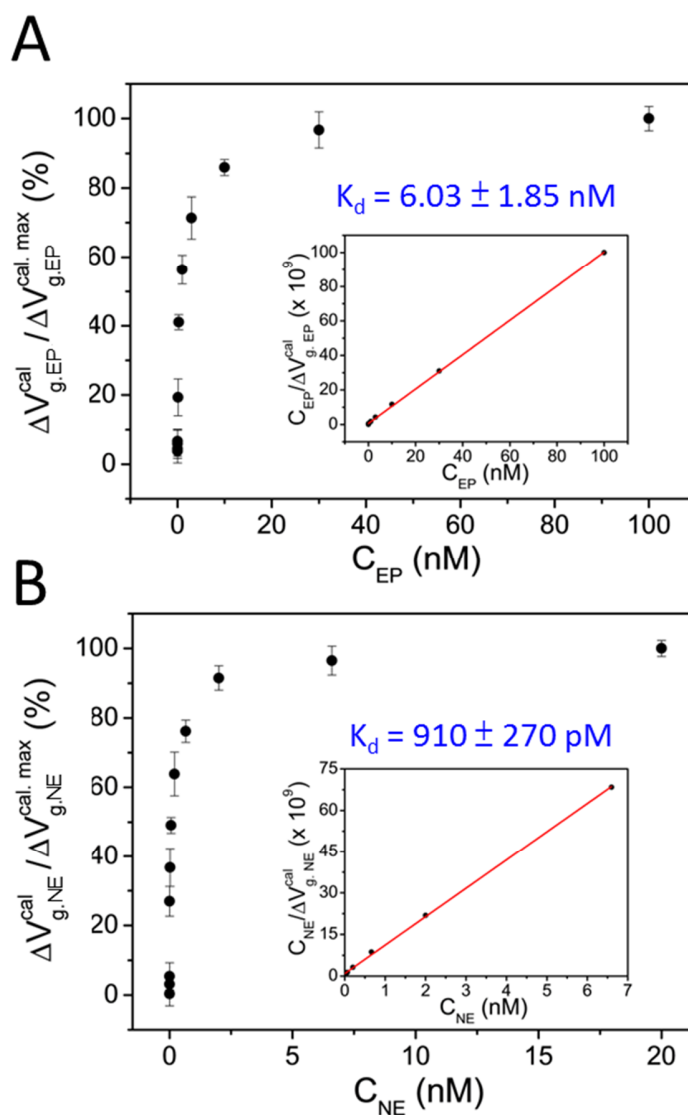


Figure S7. (A) The plot of $\Delta V_{g,EP}^{cal} / \Delta V_{g,EP}^{cal,max}$ as a function of C_{EP} . The inset shows a least-squares fit (to Eq. S1) of the measured $C_{EP} / \Delta V_{g,EP}^{cal}$ vs. C_{EP} data to yield $K_d = 6.03 \pm 1.85 \text{ nM}$ for the aptamer–EP complex. (B) Similar treatment gives $K_d = 910 \pm 270 \text{ pM}$ for the aptamer–NE complex.

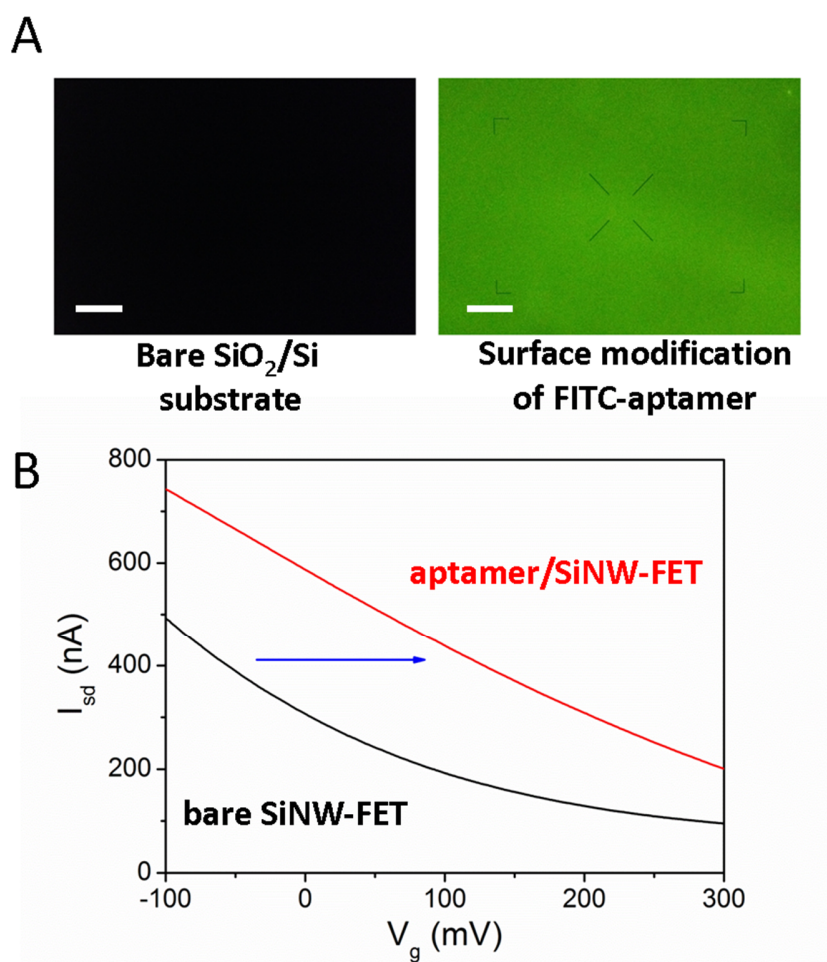


Figure S8. (A) Fluorescent images of a bare SiO₂/Si substrate and a FITC-aptamer-modified SiO₂/Si surface. (B) The I_{sd} - V_g curves measured with a bare SiNW-FET (black trace) and an aptamer/SiNW-FET (red trace) in 0.1× PBS buffer. Scale bar is 100 μ m.

REFERENCES

- (S1) Patolsky, F.; Zheng, G. F.; Lieber, C. M. *Nat. Protoc.* **2006**, *1*, 1711.
- (S2) Li, B. R.; Chen, C. W.; Yang, W. L.; Lin, T. Y.; Pan, C. Y.; Chen, Y. T. *Biosens. Bioelectron.* **2013**, *45*, 252.
- (S3) Lin, T. W.; Hsieh, P. J.; Lin, C. L.; Fang, Y. Y.; Yang, J. X.; Tsai, C. C.; Chiang, P. L.; Pan, C. Y.; Chen, Y. T. *Proc. Natl. Acad. Sci. U.S.A.* **2010**, *107*, 1047.
- (S4) Yang, Y. H.; Wu, S. J.; Chin, H. S.; Lin, P. I.; Chen, Y. T. *J. Phys. Chem. B* **2004**, *108*, 846.
- (S5) Wang, C. W.; Pan, C. Y.; Wu, H. C.; Shih, P. Y.; Tsai, C. C.; Liao, K. T.; Lu, L. L.; Hsieh, W. H.; Chen, C. D.; Chen, Y. T. *Small* **2007**, *3*, 1350.
- (S6) Lin, S. P.; Pan, C. Y.; Tseng, K. C.; Lin, M. C.; Chen, C. D.; Tsai, C. C.; Yu, S. H.; Sun, Y. C.; Lin, T. W.; Chen, Y. T. *Nano Today* **2009**, *4*, 235.
- (S7) Lin, T. Y.; Li, B. R.; Tsai, S. T.; Chen, C. W.; Chen, C. H.; Chen, Y. T.; Pan, C. Y. *Lab Chip* **2013**, *13*, 676.
- (S8) Chang, K. S.; Sun, C. J.; Chiang, P. L.; Chou, A. C.; Lin, M. C.; Liang, C.; Hung, H. H.; Yeh, Y. H.; Chen, C. D.; Pan, C. Y.; Chen, Y. T. *Biosens. Bioelectron.* **2012**, *31*, 137.
- (S9) Chen, K. I.; Li, B. R.; Chen, Y. T. *Nano Today* **2011**, *6*, 131.
- (S10) Tsai, C. C.; Chiang, P. L.; Sun, C. J.; Lin, T. W.; Tsai, M. H.; Chang, Y. C.; Chen, Y. T. *Nanotechnology* **2011**, *22*, 135503.
- (S11) Chiang, P. L.; Chou, T. C.; Wu, T. H.; Li, C. C.; Liao, C. D.; Lin, J. Y.; Tsai, M. H.; Tsai, C. C.; Sun, C. J.; Wang, C. H.; Fang, J. M.; Chen, Y. T. *Chem-Asian J.* **2012**, *7*, 2073.
- (S12) Tsai, C. C.; Hung, H. H.; Liu, C. P.; Chen, Y. T.; Pan, C. Y. *Plos One* **2012**, *7*, e33849.
- (S13) Liu, A. H.; Wei, M. D.; Honma, I.; Zhou, H. S. *Adv. Funct. Mater.* **2006**, *16*, 371.
- (S14) Hsu, M. S.; Chen, Y. L.; Lee, C. Y.; Chiu, H. T. *ACS Appl. Mater. Inter.* **2012**, *4*, 5570.
- (S15) Njagi, J.; Chernov, M. M.; Leiter, J. C.; Andreescu, S. *Anal. Chem.* **2010**, *82*, 989.
- (S16) Shi, B. X.; Wang, Y.; Zhang, K.; Lam, T. L.; Chan, H. L. *Biosens. Bioelectron.* **2011**, *26*, 2917.
- (S17) Wu, L.; Feng, L. Y.; Ren, J. S.; Qu, X. G. *Biosens. Bioelectron.* **2012**, *34*, 57.
- (S18) Mannironi, C.; DiNardo, A.; Fruscoloni, P.; TocchiniValentini, G. P. *Biochemistry* **1997**, *36*, 9726.
- (S19) Ishikawa, F. N.; Curreli, M.; Chang, H. K.; Chen, P. C.; Zhang, R.; Cote, R. J.; Thompson, M. E.; Zhou, C. W. *ACS Nano* **2009**, *3*, 3969.